A Coaxial 0.5–18 GHz Near Electric Field Measurement System for Planar Microwave Circuits Using Integrated Probes

Thomas P. Budka, *Member, IEEE,* Scott D. Waclawik, and Gabriel M. Rebeiz, *Senior Member, IEEE*

Abstract—**This paper reports on the basic theory of operation and experimental results obtained from an electric field imaging system for planar microwave circuits that employs the method of modulated scattering with monolithically integrated probes. The low-cost system is capable of mapping the normal and tangential electric field intensities and electrical phase delays above reciprocal microwave circuits in the frequency range of 0.5–18 GHz with a spatial electric field resolution of better than 100 μm. Monolithic probes incorporating silicon Schottky diodes integrated with electrically small dipole and monopole antenna scatterers on a 40-μm-thick high-resistivity silicon substrate are used. Electric field intensity and electrical phase delay images are presented for a 55-Ω coplanar waveguide line (CPW), a three-turn microstrip meander line at 8.8, 11.7, and 13.4 GHz, a microstrip coupled-line directional coupler at 10 GHz, and a microstrip patch antenna at 12.85 GHz. The results demonstrate that the modulated scattering technique is a valuable low-cost tool for microwave circuit diagnostics.**

I. Introduction

PRESENTLY, most standard testing techniques for monolithic microwave integrated circuits (MMIC's) involve on-wafer probing where the device-under-test (DUT) is contacted at several ports outside the circuit. S-parameter measurement systems have been demonstrated up to the W-band with passive probing techniques [1]. The mapping of the electromagnetic fields above a microwave circuit can be of great importance in detecting both desirable and undesirable interactions of the circuit with its surroundings. With a map of the electric field intensity above the substrate, tighter control over line lengths and losses may be obtained that may help save valuable chip real estate.

Currently, electromagnetic field mapping is possible with electrooptic sampling [2], [3], photo-emission sampling [4], electron-beam sampling [5], scanning force microscopy [6], passive detection schemes [7], and modulated scattering [8]–[13]. Electrooptic, photo-emission, and electron-beam sampling are generally time-domain methods where the electric field time waveform at each point above the circuit must be stored to generate a complete electric field image of the DUT. The latter methods (scanning force microscopy, passive detection, and modulated scattering) are frequency-domain methods where the DUT is tested at a specific frequency of interest. By using the modulated scattering technique, the direction, magnitude and phase delay of the electric fields at each position over a DUT can be determined up to very high frequencies.

Of all the electromagnetic field detection methods at present capable of measuring both electric field magnitude and phase, the easiest to implement at microwave and millimeter wave frequencies is the modulated scattering method proposed and developed in the 1950's by Richmond [8], Cullen and Parr [9], and Justice and Rumsey [10], and applied to planar microwave circuits using a 1.4–2.2-GHz coaxial system by Zürcher in 1992 [12]. Previous work by the authors [13] employed hybrid probes with physically large hybrid-mounted diodes in proof of concept tests over microstrip lines and coplanar waveguides. The physically large diode structure used in [13] was found to limit the resolution of the electric field mapping system. In this paper, the basic theory of operation of a modulated scattering experiment is presented, and an improved modulated scattering system using integrated probes is described. By monolithically integrating monopole and dipole scatterers on the same probe with planar silicon Schottky diodes, the system is pushed to higher frequencies with finer resolution. The systems currently work from 500 MHz to 2.0 GHz and from 2 to 18 GHz and can be extended for operation up to 60 GHz using a coaxially based system.

II. Modulated Scattering System

The modulated scattering method is an indirect measurement technique that locally determines the electric field intercepted by a small scattering probe in the near field of the circuit or antenna of interest. Instead of detecting the electric field directly from the probe, as with video detection, the DUT's ports are used as receiving ports for the probe's weakly scattered voltage wave. Direct detection schemes such as video detection have a low dynamic range and do not yield electric field phase information. Modulated scattering

Manuscript received August 23, 1995; revised August 26, 1996. This work was supported by the NASA/Center for Space Terahertz Technology.

T. P. Budka was with the NASA/Center for Space Terahertz Technology and the Electrical Engineering and Computer Science Department, University of Michigan, Ann Arbor, MI 48109-2122 USA. He is now with the Defense Systems and Electronics Division of the Systems Group, Texas Instruments Incorporated, Dallas, TX 75243 USA.

S. D. Waclawik was with the NASA/Center for Space Terahertz Technology and the Electrical Engineering and Computer Science Department, University of Michigan, Ann Arbor, MI 48109-2122 USA. He is now with Stanford University, Stanford, CA 94305 USA.

G. M. Rebeiz is with the NASA/Center for Space Terahertz Technology and the Electrical Engineering and Computer Science Department, University of Michigan, Ann Arbor, MI 48109-2122 USA.

Publisher Item Identifier S 0018-9480(96)08484-0.

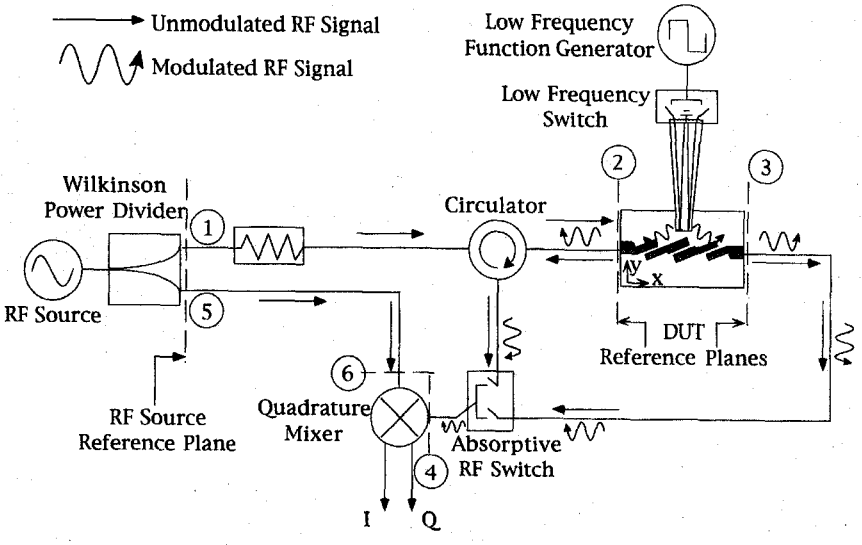

Fig. 1. The microwave circuit electric field imaging experiment using the technique of modulated scattering.

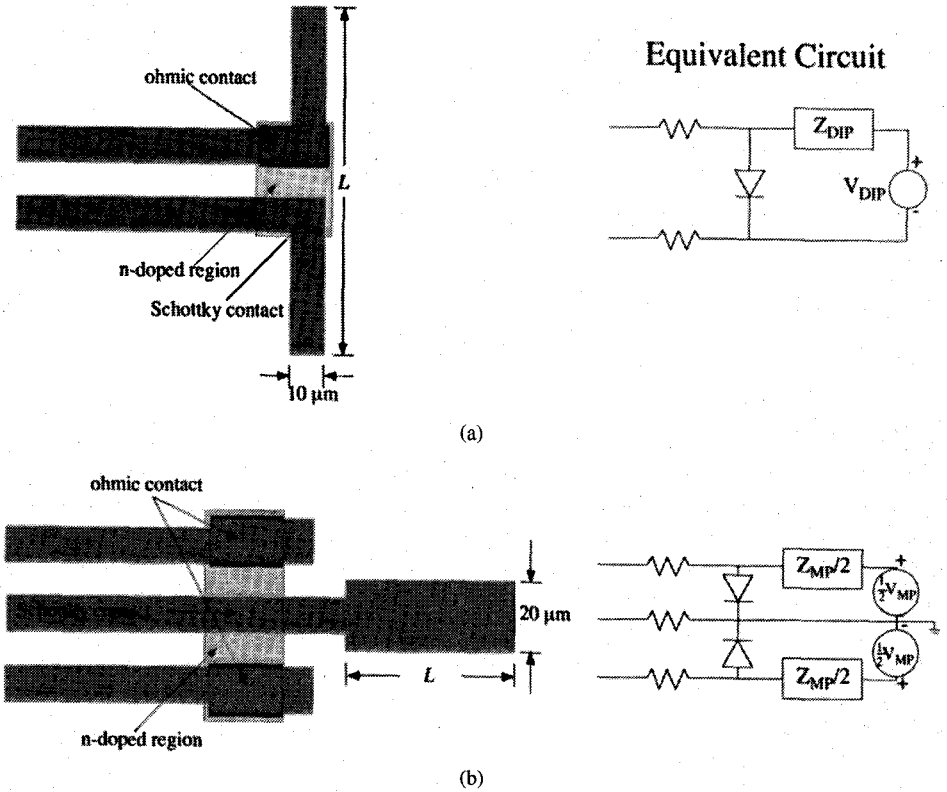

Fig. 2. (a) Integrated dipole probe and (b) integrated monopole probe that are fabricated on high resistivity silicon.

employs homodyne detection which allows for measuring greater dynamic range and phase.

A small dipole scatterer with a diode mounted at the center is placed in the near field of the circuit of interest. By modulating the bias of the diode at a frequency much lower than the radio frequency (RF), a weak modulated scattered RF signal returns to the transmitter. By using the transmitter also as a receiver, the modulated signal can be detected with little or no distortion of the near electric fields. The strength and phase of the scattered signal are directly related to the square of the normalized electric field distribution intercepted at the position of the dipole or monopole scattering probe [8].

Fig. 1 displays a schematic of the RF section of the near-field modulated scattering experiment. The power from an RF source is first divided by a Wilkinson power divider. Part of the RF signal is sent as the local oscillator (LO) to a wideband quadrature mixer from point 5 to point 6 in Fig. 1. The forward travelling RF signal passes first through an attenuator and a wideband circulator before entering the DUT. A modulated scattering probe with a diode mounted or integrated with the electrically small antenna (dipole, monopole, loop, etc.) is placed in very close proximity to the DUT at a specific position. Because the power scattered to the input/output port by the probe is very small (orders of magnitude less than the

input power to the DUT), homodyne mixing is used to detect the weakly modulated signal.

The reflected scattered signal is diverted to a wideband homodyne quadrature mixer by a wideband circulator, and the in-phase and quadrature intermediate frequency (10–100 kHz) voltages are detected by a lock-in amplifier. The signal levels from the in-phase and quadrature channels of the mixer for a typical microwave circuit with a 10-dBm input power range from 10 μV to 10 mV, when measured with a lock-in amplifier with a 10-dB gain preamplifier. Through the use of an absorptive RF switch, both the scattered reflected (input port) and scattered transmitted (output port) waves, magnitude, and phase can be detected by the same quadrature mixer. No additional filtering is needed in the circuit to attenuate undesired harmonics.

The scattering probes are mounted on a computer-controlled submicrometer translational stage. By moving the probe over a region of interest, a complete two-dimensional electric field intensity image and a phase image from the normal and tangential electric fields are collected and stored in the computer. The entire system is controlled via a personal computer with software written in "C." The system fits on an optical bench with optical rails and manual micrometers to align the probe with the microwave circuit (± 10 μm for each 10.0 mm of travel). The positioning of the probe is accomplished by the use of an X-Y submicrometer translational stage. The range of travel is limited to 25.4 mm, and the positioning accuracy is better than 0.5 μm. The speed of acquisition for a single frequency test is limited by the speed at which the probe can be positioned over the DUT.

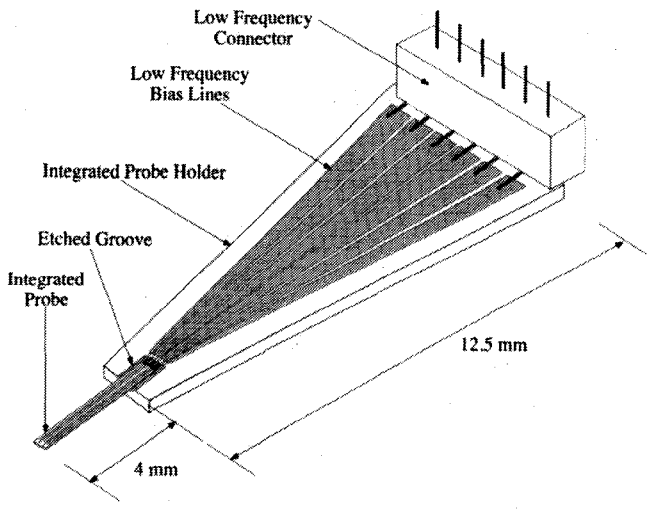

Fig. 3. Integrated probe on 40-μm thick silicon mounted on a low resistivity 500-μm thick silicon wafer with silver epoxied low frequency connector on right.

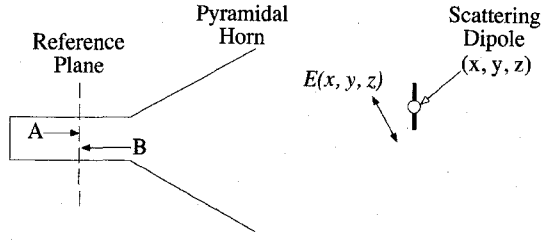

Fig. 4. Modulated scattering system for a pyramidal horn and a small dipole scatterer.

III. Monolithic Probe Design and Fabrication

The design of a probe is critical to the operation of any electric field mapping system. In this paper, monolithic probes on a 40-μm-thick silicon substrate (0.1 λ_d at 200 GHz) are used to map the electric fields over microwave circuits. Hybrid probes on 125 μm quartz wafers were initially fabricated and are described in [13]. A good probe should be as small as possible on a very thin substrate. The dipole and monopole antennas are electrically small ($\lambda_o/100 - \lambda_o/1000$) and as close to the end of the probe tip as possible. The low resistance and high capacitance of a short dipole gives a flat frequency response until the dipole approaches its first resonance at half a wavelength (2 THz for a 150-μm-long dipole in free space) [14].

Integrated probes are fabricated on a high-resistivity silicon substrate using an integrated Schottky diode as the modulating element. The fabrication process is modeled on SUPREME, a two-dimensional silicon process simulator. The dopant dose and energy are chosen to have a highly doped Schottky diode ($n^+ = 2 \times 10^{17}/cm^3$), and the ohmic contact dose is chosen to have a high shallow doping concentration of $n^{++} = 10^{20}/cm^3$. To simplify processing, aluminum is used as the Schottky metal instead of the ohmic metal. The ohmic contact relies upon tunneling as the transport mechanism.

The Schottky diodes are designed to be low resistance, low capacitance diodes that would be able to pass up to 10 mA under forward bias. The geometry of the diode is chosen to fit the 10 μm wide bias lines for both the monopole and the dipole. Both diodes turn on at approximately 0.5 V. The series resistance of a single diode is measured to be 12 Ω. The junction and parasitic capacitance (C_j+C_p) of the dipole diode is measured to be 2.0 pF, which yields a cutoff frequency of 40 GHz. Due to the high doping of the diodes, the reverse breakdown voltage is fairly low—around -3 V. This does not present a problem since the diode with be biased between -1 V and $+1.25$ V and will not intercept electric fields strong enough to force an operation in a reverse breakdown mode.

Fig. 2 displays the layout of the integrated probes. The dipole probes, fabricated with antenna arms with various lengths, $L = 150$, 250, and 350 μm. The monopole probes are 50, 100, 200, and 400 μm long. Individual probes have an overall length of 5 mm and a width of 0.5 mm. The resistive feeding transmission lines are chosen to have a characteristic impedance of 120 Ω, and they rapidly attenuate any RF signal that may propagate along the bias lines. This attenuation will minimize electromagnetic coupling of the long bias lines with the DUT.

Fig. 3 displays a completely integrated probe and holder. The probe is mounted on an anisotropically etched low-resistivity silicon wafer probe holder. A rectangular groove is etched on the holder wafer in a solution of potassium hydroxide (KOH) until an etched depth of 80 μm is reached. Gold bias lines are then patterned on the etched wafer before

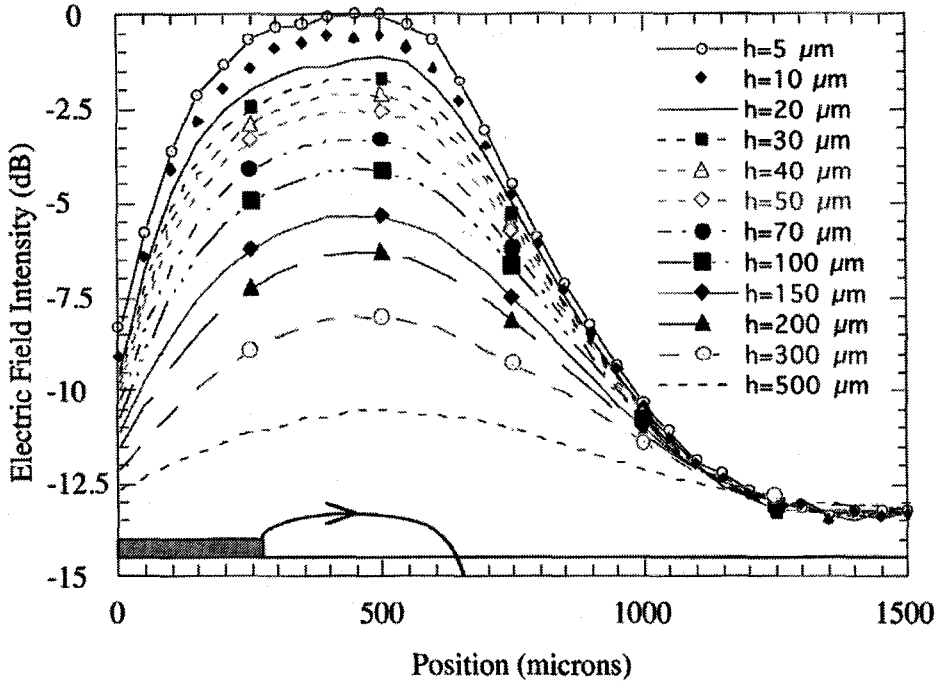

Fig. 5. Measured tangential electric field versus transverse position at selected heights above a 50-Ω microstrip transmission line ($\epsilon_r = 6.15$, $h = 0.38$ mm, $w = 0.56$ mm). The microstrip line is centered at the origin.

dicing the probe holders. To mount a probe, cyanoacrylate glue is placed in the etched groove, and the probe is placed inside the groove. The groove aids in the alignment of the probe and prevents it from moving as the thin film of glue spreads between the probe holder and the probe tip. The probes are then wire bonded with a 0.7 mil wide gold ribbon to the probe holder, and the probe holder is attached to the X-Y micropositioner.

IV. Theory of Operation and Calibration Techniques

The modulated scattering theory applied to a pyramidal horn antenna with a small scattering dipole is well known and was developed in 1955 by Cullen and Parr [9]. Fig. 4 displays the experiment. Let $\boldsymbol{A}$ be defined as a forward travelling voltage wave and B as a backward travelling voltage wave at a reference point within the waveguide. The electric field at the position of the small dipole antenna will be directly proportional to the forward travelling wave complex amplitude, $\boldsymbol{A}$, and a *normalized* electric field distribution, $\boldsymbol{F}(x, y, z)$. $\boldsymbol{F}(x, y, z)$ is unitless and does not depend on the input power into the system. This electric field at the dipole position, (x, y, z), is given by [9]

$$\boldsymbol{E}(x, y, z) = \boldsymbol{A}\boldsymbol{F}(x, y, z). \tag{1}$$

By using the reciprocity theorem, the backward travelling wave within the waveguide is derived as [9]

$$B = A\left(\frac{j\omega\alpha Z_o}{ab}\right)[\boldsymbol{u}\cdot\boldsymbol{F}(x, y, z)]^2 \tag{2}$$

where Z_o is the characteristic impedance of the waveguide, a and b are the waveguide dimensions, ω is the operating frequency, α is the polarizability of the dipole, and $\boldsymbol{u}$ is the unit vector in the direction of the dipole.

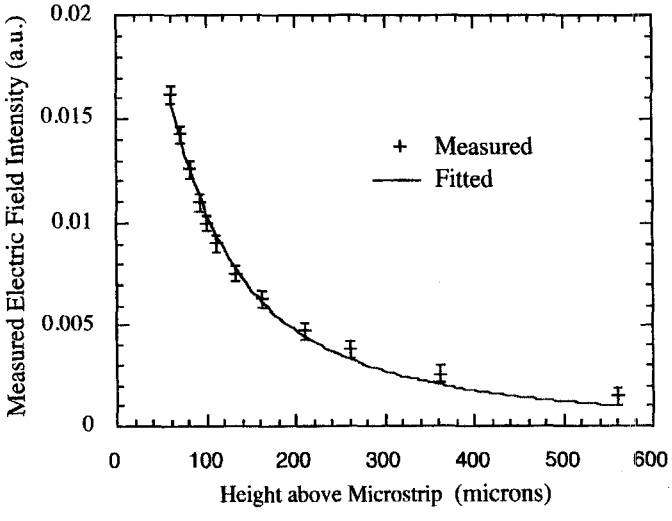

Fig. 6. Peak tangential electric field intensity versus height over a 50-Ω microstrip transmission line.

From (2), the voltage of the backward travelling wave is proportional to the square of the normalized electric field at the location of the dipole. To quote [9], "This is the fundamental formula on which the method depends."

The same argument can be applied to any reciprocal scattering process regardless of the scattering path or multipath effects as outlined for the case of two dipoles by Hygate and Nye [11] as well as for reciprocal microwave circuits as shown by Zürcher [12]. In this paper, the square of the electric field ($|E(x, y, z)|^2$) is referred to as the *electric field intensity*.

The calibration of the electric field imaging system must be divided into several types of magnitude and phase corrections. The first type will facilitate a relationship of an electric field map of a microwave circuit with a specific probe at one

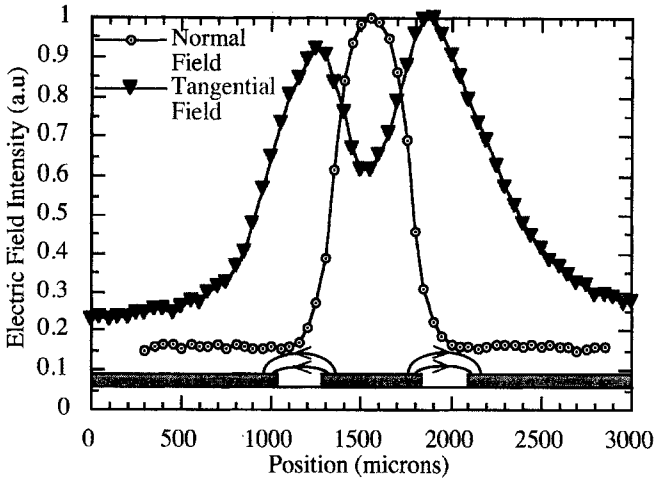

Fig. 7. Normal and tangential electric field intensity cross section over the CPW line. Each field component has been normalized to itself.

frequency with the electric field map at another frequency. For this calibration, all of the losses within the system including cable losses, insertion losses of microwave components, and conversion losses of the mixers must be measured at all frequencies of interest and factored from each measurement. Equation (3) displays the form for the magnitude of the measured voltage at the output of the quadrature mixer

$$|B| = kS_{21}S_{42}G_M|E(x, y, z)|^2. \tag{3}$$

The RF voltage conversion gain of the mixer is given by G_M, and the scattering parameters, S_{21} and S_{42}, correspond to the points labeled in Fig. 1.

To calibrate the electric field phases from one frequency to the next, a microstrip transmission line of a low dielectric constant (around $\epsilon_r = 2.2$) is used as a calibration standard. The specific probe to be used is scanned across the microstrip line, and an electric field cross section is taken at all frequencies of interest. Since the cross section of a single mode microstrip line has a constant phase, the measured phase at this reference position is stored and subtracted as an offset from the phase map.

Another type of calibration relates the scattering amplitude of the monopole probe with the dipole probe to create a complete vectorial electric field map above the circuit of interest. Both the dipole and the monopole scatter the near electric fields with differing efficiencies and add a small phase offset to the scattered microwave signal. The phase offset need not be taken into account because it will be calibrated out of the measurement from the frequency response calibration. The scattering efficiency, however, needs to be accurately determined. This type of calibration is not performed in this paper and, therefore, each electric field map is normalized to its own peak value.

V. Verification of the Method

A. Electric Field Decay Versus Height

In order to verify that the measured voltage from the in-phase and quadrature components of the quadrature mixer is truly proportional to the square of the electric field amplitude,

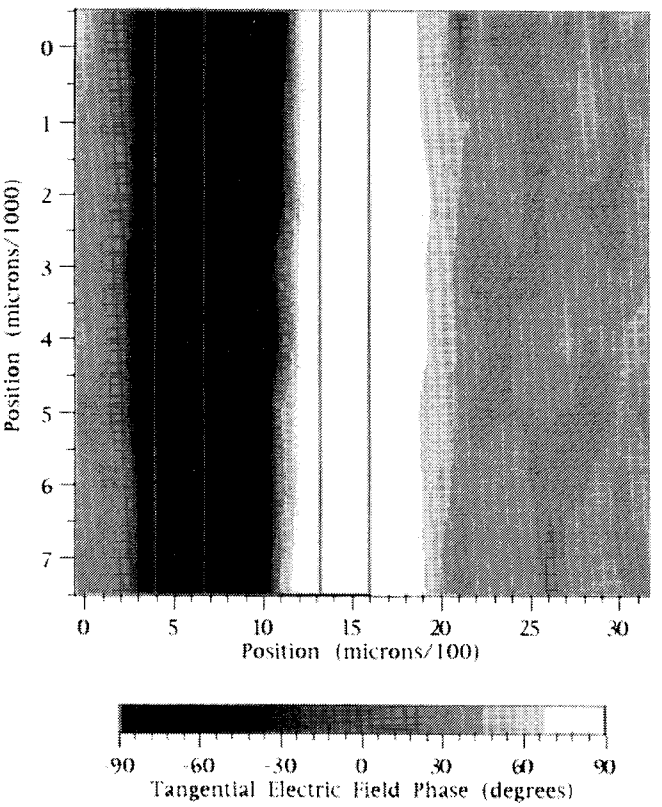

Fig. 8. Tangential electric field phase at 2.5 GHz of a coplanar waveguide transmission line terminated with an open. The phase difference across each gap is 180°.

a measurement of the electric field at various heights and positions over a 50-Ω microstrip transmission line is performed. The 50-Ω microstrip line is fabricated on Roger's Corporation RT/Duroid with a dielectric constant of $\epsilon_r = 6.15$ and a substrate thickness of $h = 0.38$ mm. The experiment is performed at 10.0 GHz with a 150-μm long dipole on a 40-μm-thick silicon substrate, with a silicon Schottky diode integrated with the dipole. Tests of the S-parameters of this 50-Ω ($S_{11} < -15$ dB) microstrip line with and without the probe contacting the line provided no observed frequency shift and no observed change in S_{11} down to -20 dB. Future work will quantify the near field interaction of the probe with the DUT.

Fig. 5 displays the measured transverse electric field intensity normalized to the peak signal at a reference height of 5 μm above the microstrip line. Because the plot is symmetric with respect to the transverse position, the plot origin is centered with the center of the microstrip line. As expected, the tangential electric field reaches its lowest value at the center of the microstrip line (the origin). The electric field does not completely reach a null due to the spatial averaging of the 150-μm-long monolithic dipole scatterer.

Fig. 6 displays the measured peak transverse electric field intensity versus height above the microstrip line. The measured values were fit to a first-order electrostatic approximation of the electric field intensity near a line of uniform charge density. The tangential electric field intensity near the edge of the microstrip should decay proportionally to $(1/h)^2$, where h is the height above the microstrip line. This model is valid to the first order until a height is reached that is nearly the

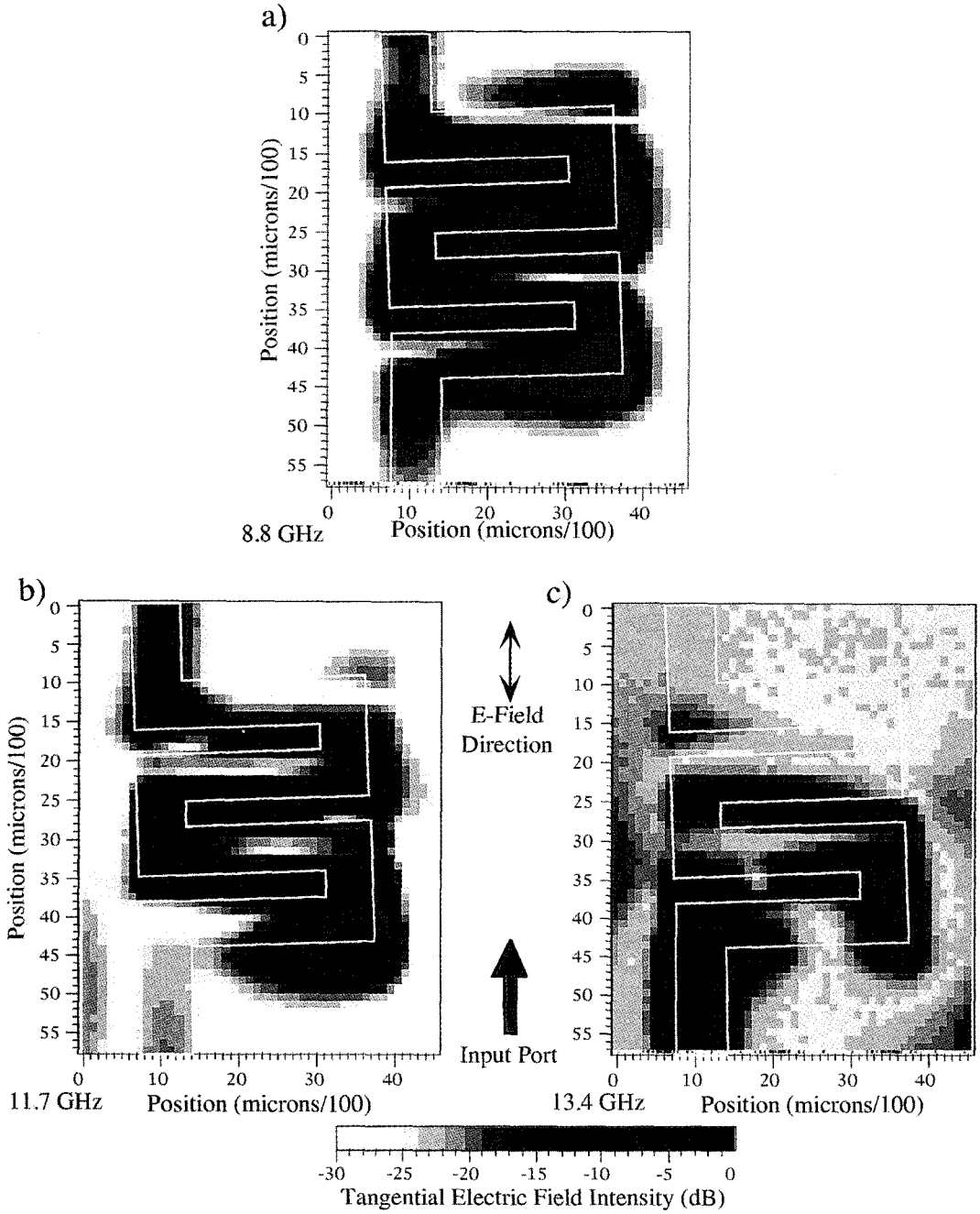

Fig. 9. Meander line measured tangential electric field at (a) 8.8 GHz (passband), (b) 11.7 GHz (edge of passband), and (c) 13.4 GHz (rejection band).

width of the microstrip line where the effects of the other side of the microstrip electric field need to be included in the approximation. From Fig. 6, it is apparent that the first-order approximation is excellent when the height is smaller than the width of the microstrip line.

The function used to fit the measured and calculated peak tangential electric field intensity contained two degrees of freedom, a variable intensity ($m2$), and a positional offset ($m1$ in micrometers). Equation (4) displays the form of the function used for the fit

$$E^2(h) = m2(m1 + h)^{-2}. \tag{4}$$

The correlation coefficient with the fitted curve is 0.997, and the peak intensity and the offset coefficient are $m2 = 448$ and $m1 = 107$ μm, respectively. The variable, $m2$, is an arbitrary scaling factor whereas the offset height, $m1$, can be interpreted as the distance from the surface of the substrate (into the substrate) of the center of rotation for the curving electric field lines. Because the microstrip line substrate thickness is 380 μm, the offset height for the curve fit is a physically reasonable value.

B. 50 Ω Microstrip Line and 55 Ω Coplanar Waveguide Line

The validity of the experimental measurements is tested with hybrid probes over a 50-Ω microstrip line and a 55-Ω CPW line in [13]. The forms of the in-phase and quadrature voltage signals along the length of a transmission line after a frequency

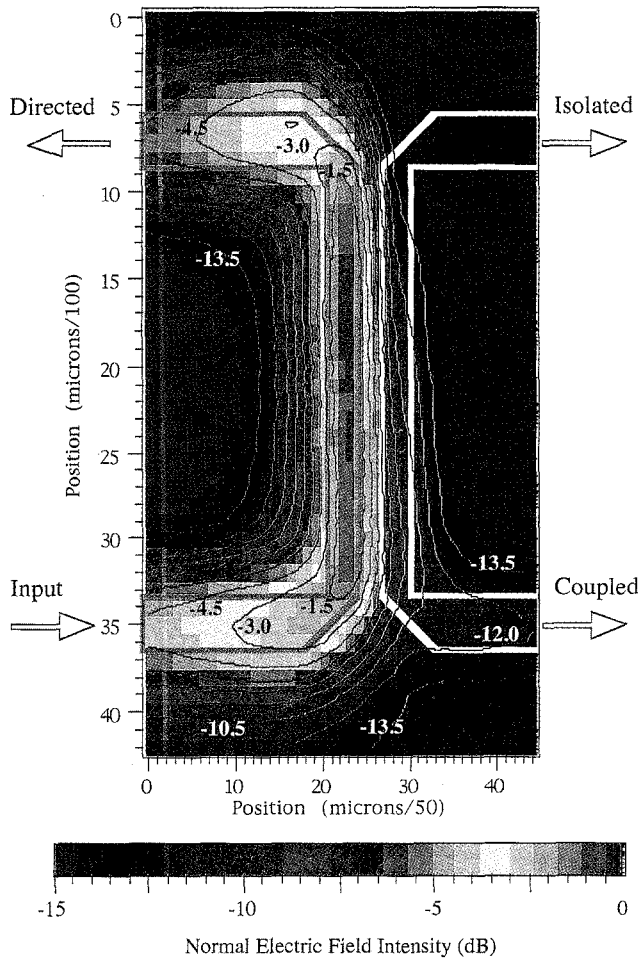

Fig. 10. Contour/intensity plot of the normal electric field intensity measured with a 100-μm-long integrated monopole scatterer at 10 GHz over a directional coupler.

calibration are given by

$$I_r = kE^2(x, y, z)\sin(\phi_o - 2\alpha_i(x, y)) = kE^2(x, y, z)\sin\left(\phi_o - 2\left(\frac{2\pi l}{\lambda_{eff}}\right)\right)$$

$$Q_r = kE^2(x, y, z)\cos(\phi_o - 2\alpha_i(x, y)) = kE^2(x, y, z)\cos\left(\phi_o - 2\left(\frac{2\pi l}{\lambda_{eff}}\right)\right) \quad (5)$$

where k is a scaling factor that contains the positionally invariant losses and other positionally invariant parameters. The positionally invariant phases have been combined into the term ϕ_o, and the positionally varying electric field is given by the term $E(x, y, z)$. $2\alpha_i(x, y, z)$ is the positionally varying round trip phase of the electric field which reduces to $2(2\pi l/\lambda_{eff})$ along the length of the transmission line. The equations predict that the maxima and minima along a transmission line for the in-phase and quadrature signals are separated by a distance of $\lambda_{eff}/4$. The in-phase and quadrature voltages are combined to result in phase and intensity measurements.

A 55-Ω CPW transmission line is fabricated and tested using Roger's Corporation RT/Duroid, $\epsilon_r = 10.8$, and a dielectric thickness of 2500 μm (100 mils). The slot width is 255 μm, and the center conductor width is 560 μm. The S-parameters are measured and modeled with LIBRA, and it is found that the characteristic impedance of the transmission line is 55 Ω. Fig. 7 displays a combined plot of the measured normal (100-μm-long integrated monopole) and tangential (150-μm-long integrated dipole) electric field intensities along a cross section of the CPW line. The normal fields peak at the center conductor and reach their lowest value across the slot of the CPW line. Additionally, the tangential electric fields peak across the slot of the CPW line and reach their lowest value over the center conductor, as expected, from simple electrostatic theory. As in the case of the microstrip line measurements, the tangential electric field does not reach a perfect null in the center of the CPW line due to finite spatial averaging effects of the dipole. The values from each electric field component are normalized to their own peak value.

Another important measurement is the phase of the electric field across the gaps of the CPW. If the CPW line is operating in the odd mode, the measured phase of the electric field across one gap should be 180° out of phase with the measured electric field phase across the opposite gap. Fig. 8 displays the tangential electric field phase measured over an *open* CPW line at 2.5 GHz with a 150-μm-long monolithic dipole scatterer. There is no phase variation along the length of the line due to the presence of standing waves, but there is an oppositely directed electric field on one side of the gap of the CPW, compared with the other side of the gap when the CPW is working in the odd-mode. When the same CPW line is measured with a 50 Ω termination at these frequencies, the phase varies linearly along the length of the transmission line, but at each cross section the phase is 180° opposite across one gap when compared with the other gap.

VI. Measurement of Microwave Integrated Circuits

C. Microstrip Meander Line

A three-turn meander line studied by Harokopus [15] is measured. The meander line is fabricated on 635-μm thick Roger's Corporation RT/Duroid with a dielectric constant of 9.9. The meander line geometry is superimposed onto Fig. 9. The meander line behaves as a low-pass filter until the path length of the meandered lines becomes long enough so that the closest lines destructively interfere with each other. From the scattering parameters, the maximum rejection occurs at a frequency of 13.4 GHz.

The tangential electric fields in the direction of the input and output microstrip lines are measured with a 150-μm-long monolithic dipole scatterer. Three frequencies are measured: 8.8 GHz (passband), 11.7 GHz (end of passband), and 13.4 GHz (rejection band). Fig. 9 displays the tangential electric field intensities at a height of 30 μm above the meander line. At 8.8 GHz, the tangential electric field intensity appears to be very uniformly distributed across the gaps of the meander line, whereas at the edge of the passband, at 11.7 GHz, the

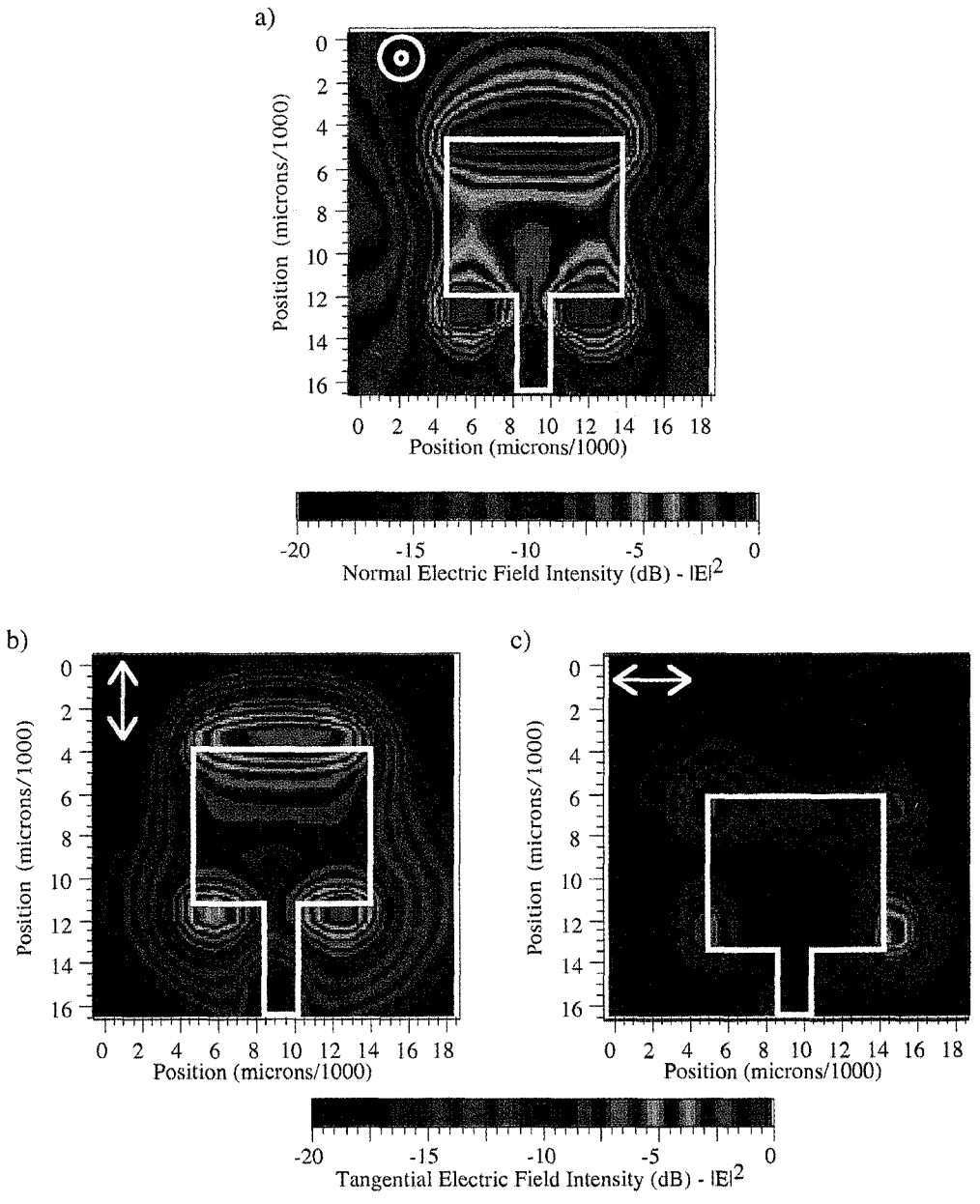

Fig. 11. Measured electric field intensities above a patch antenna at 12.85 GHz. A 200-μm-long hybrid monopole and a 250-μm-long hybrid dipole were used to measure the (a) normal, (b) vertical tangential, and (c) horizontal tangential electric field intensities.

tangential electric field becomes asymmetric and nonuniform. In the rejection band, the tangential electric field intensity across the middle gap is reduced by 15 dB from the peak intensity value. By the gap closest to the output port, the field intensities are further reduced by more than 20 dB.

D. Microstrip Directional Coupler

A single stage microstrip coupled line directional coupler is fabricated on a 380-μm-thick high-resistivity silicon substrate ($\epsilon_r = 11.7$). The layout of the directional coupler used for this experiment is superimposed over the normal electric field map presented in Fig. 10. The device is tested at 10 GHz where the measured input reflection coefficient (S_{11}) is -14 dB, the transmission to the direct port (S_{21}) is -3 dB, and the coupling (S_{31}) is -15 dB. The isolation (S_{41}) is not measured because the isolated port was terminated with a 50-Ω thin film resistor. It is expected that each SMA connector contributes 0.5 dB of loss at 10 GHz, and that the 1 cm long microstrip line on either side of the coupler contributes 0.8 dB of loss as well. After taking these initial losses into account, the directional coupler is expected to provide an internal coupling ratio of nearly -12 dB of coupling at 10 GHz.

Fig. 10 displays the measured normal electric field intensity at 10 GHz using a 100-μm-long integrated monopole. The important features of these figures are that the normal electric field is nearly constant between the input and directed port microstrip line, and that the isolated port does not appear to have a normal electric field intensity within the range of the measurements. However, the coupled port does have a normal electric field intensity that is approximately -12 dB lower than the peak normal electric field component over the input

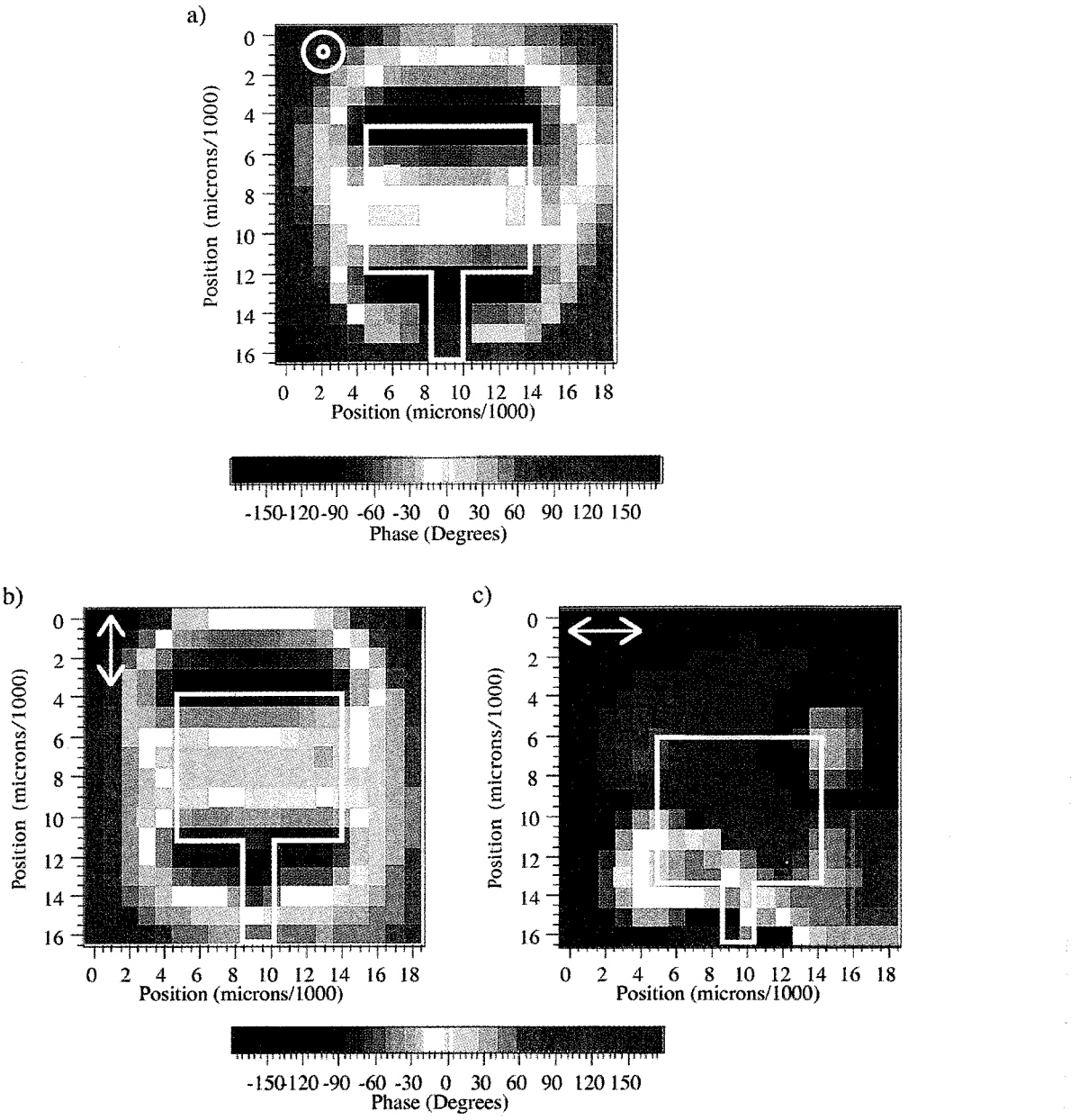

Fig. 12. Measured round trip electrical phase delay of the (a) normal electric field, (b) vertical tangential electric field, and (c) horizontal tangential electric field.

microstrip line, which agrees well with measured S-parameter values.

E. Microstrip Patch Antenna

A microstrip patch antenna is fabricated on Roger's Corporation RT/Duroid ($\epsilon_r = 2.2$, $h = 0.635$ mm) and tested at the first resonance frequency of 12.85 GHz. The patch antenna's width is 9120 μm, the length is 7410 μm, and the input microstrip line width is 1960 μm. The edges that are perpendicular to the microstrip input line are the radiating edges of the microstrip patch antenna. By using the modulated scattering system with hybrid probes (a 250-μm-long dipole and a 200-μm-long monopole), all electric field component intensities and phases are measured.

Fig. 11 displays the measured electric field intensities that are collected with a spacing of 1000 μm in each direction. Because the electric fields around the patch antenna do not change very rapidly with position, this spacing is adequate to display the radiating characteristics of this type of antenna. As predicted, the radiating edges of the patch have the strongest electric field components in the normal (a) and tangential (vertical) (b) directions. The nonradiating electric field component in the horizontal direction (c) has a much lower intensity than the vertical electric field component (b) and has nulls at the center of each edge of the patch antenna. Another interesting feature is that the fields are very strong in the substrate beyond the edge of the patch antenna in (a) and (b). By using the modulated scattering system, the near electric fields of planar antennas may be mapped at any distance away

from the surface. Fig. 12 displays the round trip electrical phase delay from the input port to the probe's position above the patch antenna at 12.85 GHz. As expected, the normal field phase delay (a) the tangential (vertical) field phase delay are constant across the radiating edges of the patch antenna. The nonradiating tangential (horizontal) field phase delay is 180° out of phase with respect to each corner of the patch antenna.

VII. Discussion and Conclusions

In this paper an experimental electric field imaging system that uses the method of modulated scattering is presented. The system follows the method used by Zürcher [12] and improves upon the techniques used by Richmond [8] in that the system is completely coaxial. By using standard semiconductor processing techniques to make integrated Schottky diodes with the scattering antennas, the size of the probes used in this research is more than 50 times smaller than commonly used probes.

Many applications for this research exist for nonreciprocal devices such as amplifiers, digital phase shifters, mixers, etc. as well as for quasioptical testing of complex radiating circuits such as log periodic and spiral antennas. Knowledge of the electric fields over these circuits will allow the determination of the propagation constants, device-to-device coupling, and the losses and the existence of substrate and evanescent modes. This information can be used for the placement of more circuitry within the same area and will speed the circuit debug-time during the developmental stages.

Overall, the most important benefit of the modulated scattering technique is the system's adaptability to test a wide variety of circuits on different substrates (Roger's Corporation R/T Duroid, quartz, silicon, gallium arsenide, etc.). The system is modular and can be very easily changed to test new circuits of interest. Any probe configuration is possible as long as the probe contains a modulating element. Although loop antennas which are sensitive to the magnetic field are not developed in this work, they could also be used with the modulated scattering technique. Higher frequency RF components can be used to extend the operation of the modulated scattering system up to 60 GHz for a coaxially based system.

Future efforts will apply the technique toward higher operating frequencies and will work on improving the sensitivity, dynamic range, and spatial resolution of the current system. Further improvements also need to be made with the phase measurements of the system. The ultimate goal would be to produce the true electric field phases at each position for each electric field component. The phase results presented in this paper are round trip electric phase delays (for the input port) and have not been converted to the true electric field phase due to the difficulty involved in this type of conversion for complex circuits. Also, signal processing software could be used for image enhancement, especially when the electric field spatial distribution varies slowly over the circuit.

Acknowledgment

The authors would like to thank Roger's Corporation for their generous donations of RT/Duroid that were used in numerous microwave test circuits for this research.

References

[1] E. M. Godshalk, "A W-band wafer probe," *IEEE MTT-S Dig.*, pp. 171–174, 1993.
[2] W. Mertin, C. Bohm, L. J. Balk, and E. Kubalek, "Two-dimensional field mapping of amplitude and phase of microwave fields inside a MMIC using the direct electrooptic technique," *IEEE MTT-S Dig.*, pp. 1597–1600, 1994.
[3] G. David, W. Schroeder, D. Jäger, and I. Wolff, "2D electrooptic probing combined with field theory based multimode wave amplitude extraction: A new approach to on-wafer measurement," *IEEE MTT-S Dig.*, pp. 1049–1052, 1995.
[4] J. Bokor, A. M. Johnson, R. H. Storz, and W. M. Simpson, "High-speed circuit measurements using photoemission sampling," *Appl. Phys. Lett.*, vol. 49, no. 4, pp. 226–228, July 1986.
[5] J. T. L. Thong, "Transit time effect in electron beam testing voltage measurements," *Meas. Sci. Tech.*, vol. 3, pp. 827–837, 1992.
[6] C. Böhm, C. Roths, and E. Kubalek, "Contactless electrical characterization of MMIC's by device internal electrical sampling scanning-force-microscopy," *IEEE MTT-S Dig.*, pp. 1605–1608, 1994.
[7] Y. Gao and I. Wolff, "A miniature magnetic field probe for measuring fields in planar high-frequency circuits," *IEEE MTT-S Dig.*, pp. 1159–1162, 1995.
[8] J. H. Richmond, "A modulated scattering technique for the measurement of field distributions," *IRE Trans. Microwave Theory Tech.*, vol. MTT-3, pp. 13–15, 1955.
[9] A. L. Cullen and J. C. Parr, "A new perturbation method for measuring microwave fields in free space," *Proc. Inst. Elect. Eng.*, pt. 3, vol. B, 102, pp. 836–844, 1955.
[10] R. Justice and V. H. Rumsey, "Measurement of electric field distributions," *IRE Trans. Microwave Theory Tech.*, vol. AP-3, pp. 177–180, 1955.
[11] G. Hygate and J. F. Nye, "Measuring microwave fields directly with an optically modulated scatterer," *Meas. Sci. Tech.*, vol. 1, pp. 703–709, 1990.
[12] J. Zürcher, "A near field measurement method applied to planar structures," *Microwave Eng. Eur.*, pp. 43–51, June/July, 1992.
[13] T. P. Budka and G. M. Rebeiz, "A microwave circuit electric field imager," *IEEE MTT-S Dig.*, pp. 1139–1142, 1995.
[14] M. Kanda, "Standard probes for electromagnetic field measurements," *IEEE Trans. Antennas Propagat.*, vol. 41, pp. 1349–1364, Oct. 1993.
[15] W. P. Harokopus, "High frequency characterization of open microstrip discontinuities," Ph.D. dissertation, Univ. Michigan, Ann Arbor, 1991.

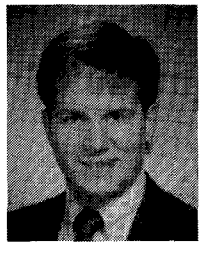

Thomas P. Budka (S'92–M'96) received the A.B. degree in physics from Dartmouth College, Hanover, NH in 1989, the M.A. degree in physics from The University of Rochester, Rochester, NY, in 1991, and the Ph.D. degree in electrical engineering from the Department of Electrical Engineering and Computer Science, The University of Michigan, Ann Arbor, in 1995.

While at The University of Michigan, he developed a low-cost electric field scanning system for mapping the electric fields above microwave circuits. He won first place in the student paper competition at the *1995 IEEE Microwave Theory and Techniques Symposium* for this research. He also developed a 75-110 GHz quasioptical amplifier which delivered 15.5 dB gain at 102 GHz. In 1995, he joined the Defense Systems and Electronics Division of the Systems Group at Texas Instruments Incorporated in Dallas, TX. His current research interests include MMIC electric field mapping techniques, electromagnetic analysis and design of novel GaAs MMIC structures, multilayer microwave circuits, packaging and high-speed interconnect design. He is also President of RF Diagnostics, which is further developing low cost MMIC diagnostics based on the work presented in this paper.

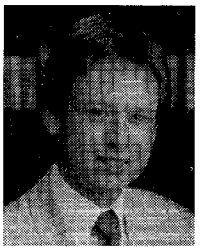

Scott D. Waclawik received the B.S. degree in electrical engineering from The University of Michigan, Ann Arbor, in 1996. He has received a National Science Foundation Fellowship and plans to attend Stanford University, Stanford, CA.

He was an intern for Motorola in the summer of 1996.

Gabriel M. Rebeiz (S'86–M'88–SM'93) received the Ph.D. degree in electrical engineering from the California Institute of Technology, Pasadena, in June 1988.

He joined the faculty of The University of Michigan, Ann Arbor, in 1988, and was promoted to Associate Professor in 1992. He was a Visiting Professor at Chalmers University of Technology, Göteborg, Sweden, in 1992, and a Visiting Professor at the Ecole Normale Superieur in 1993. He is the author of 62 papers published in refereed journals and more than 110 papers presented at national and international conferences. His interests are in applying micromachining techniques in silicon and GaAs for the development of low-loss and low-cost microwave antennas, components, and subsystems for wireless applications and satellite communication systems. He is also interested in the development of mm-wave high-efficiency antennas, planar collision-avoidance sensors for automotive applications, millimeter-wave imaging and phased arrays, and monopulse tracking systems.

Dr. Rebeiz received the National Science Foundation Presidential Young Investigator Award in 1991 and the URSI International Isaac Koga Gold Medal Award for Outstanding International Research in 1993. He also received the Research Excellence Award in 1995 from the University of Michigan. Together with his students, he is the winner of best paper awards at JINA '90, IEEE-MTT '92, '94, '95, and IEEE-AP '92 and '95. He is an elected member of URSI-D.